Ultra-high Flux Alkali-treated Cellulose Triacetate/Cellulose Nanocrystal Nanocomposite Membrane for Pervaporation Desalination

Indah Prihatiningtyas[*,1,2], Yusak Hartanto[3] and Bart Van der Bruggen[*,1,4]

[1]*Department of Chemical Engineering, KU Leuven, Celestijnenlaan 200F, B-3001, Leuven, Belgium*

[2]*Department of Chemical Engineering, Mulawarman University, Jalan Sambaliung No.9, Sempaja Selatan, Samarinda, Kalimantan Timur, Indonesia*

[3]*Materials and Process Engineering (iMMC-IMAP), UC Louvain, Place Sainte Barbe 2, 1348 Louvain-la-Neuve, Belgium.*

[4]*Faculty of Engineering and the Built Environment, Tshwane University of Technology, Private Bag X680, Pretoria 0001, South Africa*

*Corresponding authors:

E-mail: bart.vanderbruggen@kuleuven.be; indahprihatiningtyas.yamsidi@kuleuven.be

Highlights

- Alkaline post-treatment significantly boosted the hydrophilicity of CTA/CNCs membranes.
- Alkaline post-treatment enhanced the performance of CTA/CNCs membranes.
- 30 minutes is the optimum time for alkaline treatment of CTA/CNCs membranes.
- Alkali-treated membrane was able to handle highly saline water without losing its selectivity

Abstract

Cellulose triacetate/cellulose nanocrystals (CTA/CNCs) nanocomposite has recently been proposed as a promising material to synthesize pervaporation desalination membrane. However, the water flux of such membranes was found poor in comparison to other pervaporation desalination membranes. In this work, time-controlled alkaline treatment is proposed to improve the water flux of CTA/CNCs nanocomposite film membrane without compromising its selectivity. An understanding how alkaline treatment changed the physicochemical properties of the film membranes was obtained through film membrane characterization by FTIR spectroscopy, X-ray diffraction, scanning electron microscopy (SEM), contact angle and water uptake analysis. The film membrane being treated up to 30 minutes results in a drastic water flux improvement to 107.5 $kg.m^{-2}.h^{-1}$ with >99.8% salt rejection in comparison with the water flux obtained by the untreated film membrane, 3.6 $kg.m^{-2}.h^{-1}$, when hypersaline water with 90 g/L NaCl was employed as the feed solution. The water flux decreased to 58.5 $kg.m^{-2}.h^{-1}$ when 200 g/L NaCl was used as feed solution. The alkali-treated film membrane showed a stable film membrane performance for 12 hours when it was evaluated for 90 g/L and 200 g/L NaCl.

Keywords: Alkaline treatment, hypersaline water, pervaporation, desalination, cellulose nanocrystals

1. Introduction

Membrane-based desalination is a promising technology to augment fresh water supplies. Pressure-driven reverse osmosis (RO) is currently the forefront seawater desalination technology due to the absence of a phase change during the separation process, making this technology highly energy efficient and cost-effective in providing potable water compared to thermal-based desalination processes [1]. The state-of-the-art RO membrane is a thin-film composite membrane, comprising a porous polymer support with a thin film of polyamide prepared via interfacial polymerization deposited on top of this support [2]–[4]. The real game-changer has been the use of highly efficient pressure recovery systems for RO. However, this type of membrane is prone to fouling due to the intrinsic properties of polyamide materials. Furthermore, RO desalination has a limited water recovery and thus a large volume of brine is generated, which needs further treatment before being discharged to the environment [5]. Although there has been an interest in applying high pressure reverse osmosis (HPRO) desalination to treat high salinity feed streams [6], RO membranes have limited water recovery due to the very high osmotic pressure of the feed solution.

In recent years, alternative membrane-based desalination processes, such as hybrid processes making use of forward osmosis (FO), and membrane distillation (MD), have been studied as alternatives to RO desalination due to their excellent potential in handling high salinity streams. Unfortunately, FO requires much energy to re-concentrate the diluted draw solution [7] while membrane wetting and a high fouling propensity are inherent drawbacks of MD [8]. Pervaporation desalination is recently proposed as an emerging membrane desalination technology addressing several drawbacks of MD in dealing with high salinity streams. Instead of porous hydrophobic membranes, pervaporation desalination uses a dense hydrophilic membrane to perform desalination. The application of dense membranes results in a very high salt selectivity. The hydrophilic membrane surface also diminishes the fouling problems encountered in MD. However,

the low membrane water permeability is a major hurdle for desalination by pervaporation [9].

Currently, there are two types of pervaporation desalination membranes: dense symmetric and thin-film composite (TFC) membranes. The former are prepared via solution casting followed by solvent evaporation, while the latter are usually prepared by interfacial polymerization or solution coating to deposit a highly selective salt rejection layer on top of a porous polymer support. Developing high performance membranes by improving the water transport rate inside the polymer matrix while maintaining a high salt selectivity is currently the major research focus in pervaporation desalination. One of the strategies to achieve this goal is to incorporate nanofillers inside the polymer matrix for dense or TFC membranes, to prepare nanocomposite membranes with improved water permeance. Various nanomaterials have been investigated to prepare nanocomposite membranes for pervaporation desalination applications, such as SiO_2 [10]–[12], TiO_2 [13]–[15], Al_2O_3 [16], [17], graphene oxide (GO) [18]–[20], and cellulose nanocrystals [21], [22]. It has been showed that the incorporated nanofillers were able to significantly increase the water permeability due to the availability of additional water passages inside the polymer matrix. Furthermore, the mechanical properties of nanocomposite membranes are usually improved compared to their pristine version, considering that these membranes are usually very thin.

Cellulose nanocrystals are an emerging nanomaterial that has inherent hydrophilicity due to the presence of hydroxyl, sulfonic acid and carboxylic acid functional groups on its surface. It is one of the emerging nanofillers to prepare nanocomposite membranes for water desalination applications. In this work, alkali-treated cellulose triacetate/cellulose nanocrystal nanocomposite film membranes were prepared and evaluated in desalination by pervaporation. The prepared film membranes were systematically characterized to reveal the effect of alkaline treatment on film membrane physicochemical properties and performance. Optimizing the alkaline treatment time

of these nanocomposite membranes allowed to significantly enhance water flux without compromising the salt selectivity. The optimized film membrane were applied to handle high salinity feed and had a stable performance during 12 hour pervaporation experiments.

2. Experimental

2.1. Materials

Cellulose triacetate (CTA, acetyl content 43 - 44%, molecular weight 966.845 g/mol, Acros Organics TM) was used as the polymer matrix. Cellulose nanocrystals with an aggregated particle size of 1- 50 µm, the diameter of 2.3- 4.5 nm and the length of 44-108 nm as reported by the supplier, were obtained from CelluForce Inc. (Canada). Sodium chloride (NaCl) (99.5%) from Acros was employed as the solute in the feed solution. Sodium hydroxide (NaOH) was purchased from Fisher scientific, UK. All chemicals were used without further purification.

2.2. Membrane preparation

The CNCs suspensions were prepared by dispersing 3 wt.% CNCs (calculated based on dope solution weight) in DMSO as a solvent. The suspension was mixed with a magnetic stirrer for three hours at 40 °C. Subsequently, 6 wt.% CTA was loaded to the CNCs suspensions and the mixture was stirred for 15 hours. The casting dope solution was left for an hour and was centrifuged for 4 minutes at 4,000 rpm to remove bubbles generated from stirring process. The polymer films were prepared by casting the dope solution on the glass plate using an automatic casting device with a blade height of 200 µm at room temperature and a relative humidity of 34 - 44 %. The wet polymer films were left in a vacuum oven for four hours at 60 °C and 0.17 bar to evaporate the solvent. The dried film membranes were detached from the glass plate by immersing them into a water bath.

2.3. Alkaline treatment

A sodium hydroxide (NaOH) solution with a concentration of 2 M was prepared by dissolving in deionized water with a final pH of 13.25. Alkaline treatment of the film membranes was conducted by immersing the film membrane in the solution for different time periods, i.e., 6, 20, 30, and 60 minutes. The film membranes were then directly evaluated in the pervaporation setup after the alkaline treatment. The detailed steps supplied with photos can be seen in Figure S2.

2.4. Membrane characterization

2.4.1. Morphological characterization

The surface and cross-section morphologies of pristine and alkali-treated CTA/CNCs nanocomposite film membrane were characterized using a scanning electron microscope (SEM) (Philips XL30 SEM, the Netherlands). For surface analysis of the pristine CTA/CNCs nanocomposite film membrane with thickness 10 μm, the dried film membrane samples were cut in small pieces, and then pasted on the SEM holder while the samples for cross-section analysis were prepared by immersing the film membranes in liquid nitrogen followed by fracturing the film membranes before putting them onto the SEM holders. For sample preparation of alkali-treated film membranes, the samples were cut with size 4 x 4 cm, then immersed in the 2M NaOH solution at different times (6, 20, 30, and 60 minutes). Then the samples were immersed in DI water for 30 seconds to remove the remaining NaOH solution on the membrane. The treated film membrane was directly cut into small pieces and pasted on the SEM holder for surface characterization. For cross-section characterization, the treated film membranes were immersed in liquid nitrogen and fractured before pasting them onto the SEM holder.

2.4.2. X-ray diffraction (XRD)

X-ray diffraction analysis was employed to probe the structural changes of CTA/CNCs nanocomposite film membranes after the alkaline treatment. X-ray diffraction model Philips PW1830 diffractometer was used with Bragg/Brentano θ–2θ setup, CuKα radiation at 45kV - 30 mA on 173 mm goniometer circle, within the scan range of 3–75°(Rietveld users), for 1 hour.

2.4.3. FTIR analysis

The chemical composition of the untreated CTA/CNCs nanocomposite film membrane and alkali-treated film membranes was characterized using attenuated total reflectance-Fourier transform infrared spectroscopy (ATR-FTIR, Perkin Elmer, spectrum 100, USA). At least 64 scanning for each sample were conducted in the span range of 4000-650 cm^{-1}.

2.4.4. Water uptake measurement

Water uptake measurement was conducted to study the effect of alkaline treatment on the swelling properties of the nanocomposite film membranes. The film membranes were cut into a diameter of 6 cm and were immersed in DI water at room temperature for two days to reach equilibrium condition. The wet film membranes were wiped with a tissue to remove unabsorbed water before weighing to obtain the mass of wet film membranes (M_w). Next, the film membranes were dried in the oven at 105°C for one day to evaporate the adsorbed water and were weighed to obtain the mass of dried film membrane (M_d). Triplicate measurements were done for each film membrane to ensure accuracy. The water uptake of the film membranes was calculated according to the following equation.

$$Water\ uptake\ (\%) = \frac{M_w - M_d}{M_d}\ x\ 100\% \quad (1)$$

2.4.5. Pervaporation experiment

The performance of CTA/CNCs nanocomposite film membranes (pristine and alkali-treated film membranes) for pervaporation desalination was evaluated using a laboratory scale setup shown schematically in Figure 1. A feed solution was prepared by dissolving NaCl in water and poured into the feed tank. The feed solution was then heated until a predetermined operating temperature was reached. The liquid feed was circulated with a peristaltic pump into the film membrane module (membrane area was 19.625 cm^2) with a flow rate of 70 - 80 L/h. A vacuum pump with low pressure (below 1 mbar) was employed on the permeate side to generate vapor pressure difference across the film membrane. The permeating vapor was collected and condensed with a double U glass tube immersed in liquid nitrogen acting as the cold trap. The collected permeate was weighed during 3 h pervaporation process.

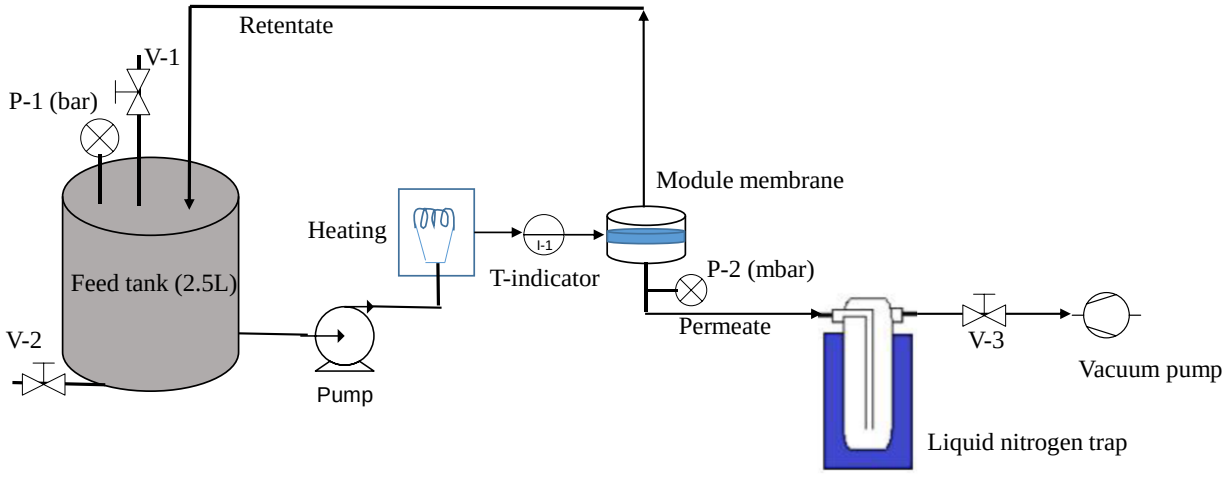

Figure 1. Schematic flow chart of laboratory scale for pervaporation desalination.

The water flux, J (kg m^{-2} h^{-1}) and salt rejection, R (%) of the pervaporation membranes were calculated using the following equations:

$$Water\ flux\ (J) = \frac{m}{(A\ x\ t)} \quad (2)$$

$$Rejection\ (\%) = \frac{(Cf - Cp)}{Cf}\ x\ 100\% \quad (3)$$

where m is the mass of the collected permeate (kg), A is the effective membrane area (m^2), t is the time period required to collect a certain amount of permeate (h), C_f is the salinity in the feed side and Cp is salinity the permeate solution. The salinity value was determined by a conductivity meter model Consort-C831.

3. Results and discussion

3.1. Membrane characterization

3.1.1. Morphological characterization

The SEM images displaying the surface structure of the untreated and alkali-treated CTA/CNCs pervaporation film membrane are shown in Figure S3. The figures show that the pristine as well as the alkali-treated nanocomposite film membranes have a dense structure. The digital images of CTA/CNCs nanocomposite untreated and alkali-treated are shown in Figure S1. Figure S1a shows that the untreated CTA/CNCs nanocomposite is dry and rigid while Figure S1b shows that CTA/CNCs film membrane after 30 minutes treatment in 2 M of solution NaOH was wet and soft.

The alkaline treatment also affects the cross-section morphology of the CTA/CNCs nanocomposite film membrane, as shown in Figure 2. Figure S5a shows that the film membrane floated on the NaOH solution. However, the membrane was slightly drowned in the solution after 20 minutes immersion (see Figure S5b), hence the alkali process is not only occurring on the film membrane surface but also in the film membrane cross section. Figure 2a shows that the cross-section of the untreated film membrane has a layered porous structure. The cross-section structure seems denser after 20 minutes of alkaline treatment (see Figure 2b); the structure more compact and dense after being treated in alkaline environment for 30 minutes (see Figure 2c). After 30 minutes in alkali solution, the film membrane pores also appear to be collapsed due to the

deacetylation process, which is in agreement with the literature [23].

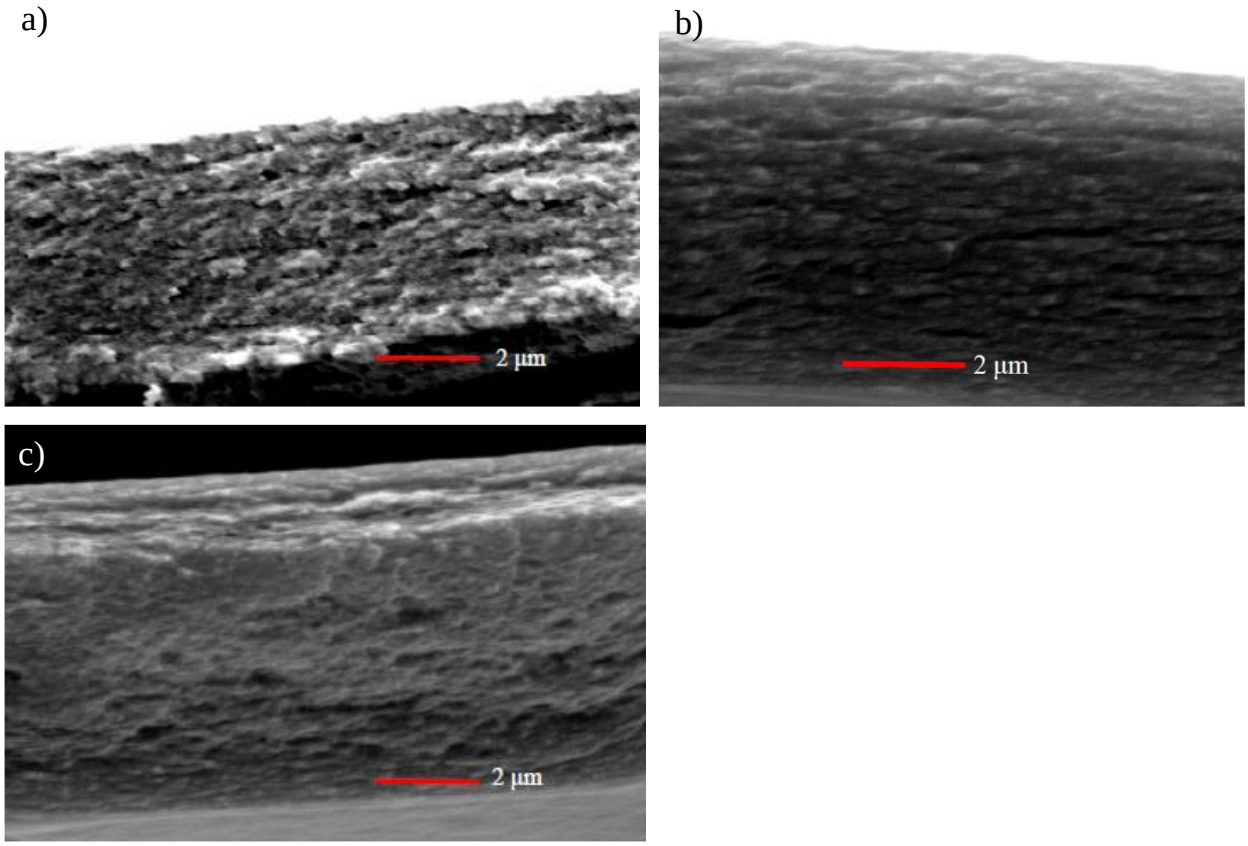

Figure 2. SEM images of film membrane cross-section: a) Untreated, b) 20 minutes of alkaline treatment, and c) 30 minutes of alkaline treatment.

3.1.2. XRD

Figure 3 describes the X-ray diffraction results of the CTA/CNCs nanocomposite film membrane at different times of alkaline treatment. The characteristic peaks of cellulose generally appear around 15°, 22°, and 35° [24]. The XRD spectrum for the untreated film membrane, as shown in Figure 3a, indicates the characteristic peak of cellulose triacetate around 5° to 10° due to acetylation of cellulose [24]. However, these peaks disappear for the alkali-treated CTA/CNCs film membrane (see Figure 3b-e). The crystalline structure of CTA/CNCs film membrane was investigated based on the commonly used crystalline peak of cellulose, i.e., around 22°. Figure 3b

depicts that the crystalline structure of the CTA/CNCs nanocomposite film membrane decreased after being alkali-treated for 6 minutes. However, an increasing alkaline treatment time, starting at 20 minutes, increases the crystalline structure of the film membrane again (see Figure 3c-e). This increase might be due to the cellulose recrystallization [25]. Alkaline treatment is able to enhance the crystal size and crystalline index of cellulose [26], [27] due to the removal of lignin [27]. Furthermore, Santos et.al reported that alkaline treatment with NaOH in hot water at 75° C enhanced the crystalline index of the piassava fibers with a decrease of the amorphous phase [28].

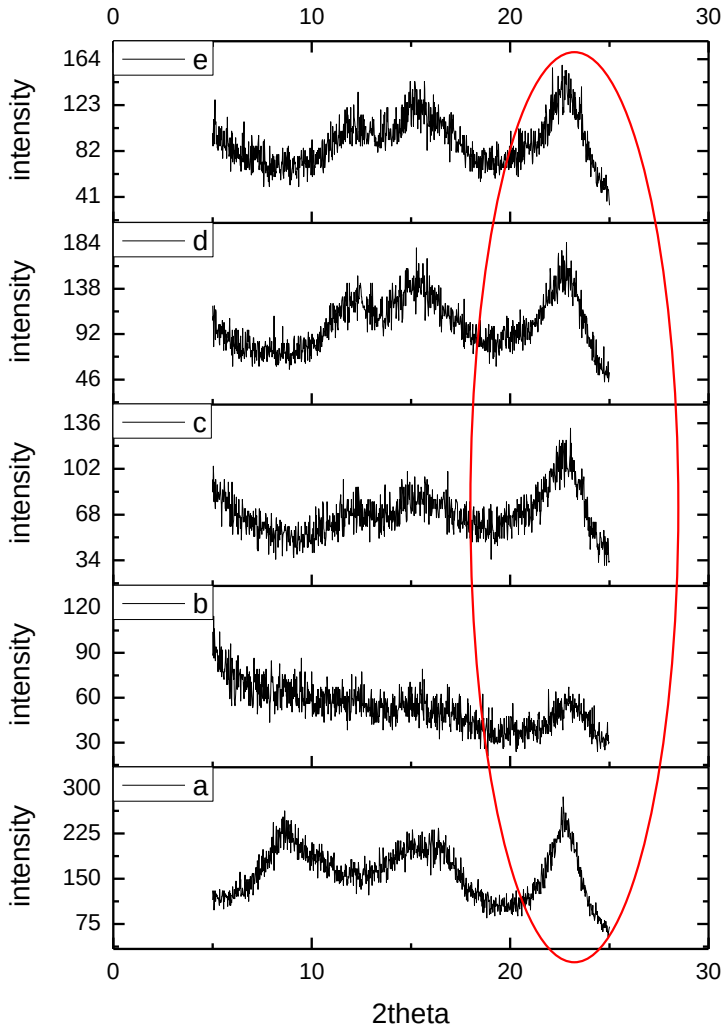

Figure 3. X-ray diffraction at different times of alkaline treatment : a) Untreated, b) 6 minutes, c)

20 minutes, d) 30 minutes, and d) 60 minutes.

3.1.3. FTIR characterization

FTIR spectra of the untreated and alkali-treated of CTA/CNCs nanocomposite film membranes are shown in Figure 4. The functional groups in Figure 4a appear as a peak at 3328 cm^{-1} referring to O-H stretching, while the peak at 2891 cm^{-1} relates to the stretching of aliphatic C-H bonds. Figure 4b shows the bands at 1744 cm^{-1}, 1643 cm^{-1}, and 1365 cm^{-1} attributed to the C=O stretching, the C=C stretching, and the asymmetric bending of C−H, respectively [21], [28]. The peaks at 1220 cm^{-1} and 1034 cm^{-1} correspond to C−O stretching and the pyranose ring C−O−C [21], while the band at 897 cm^{-1} is corresponding to the β-glycosidic linkages of the glucose ring, which it is a typical structure of cellulose [27], [28]. The spectrum after alkaline treatment as presented in Figure 4a suggests that the peak intensity at 3328 cm^{-1} has an increasing trend. This trend indicates the enhancement of O-H groups due to the deacetylation process, as shown in Figure 5, which substitutes the acetate groups with the hydroxyl groups. The enhancement of O-H groups shows that the hydrophilicity of the CTA/CNCs nanocomposite film membrane increased after alkaline treatment. However, the peak at 1220 cm^{-1} (C-O) and 1744 cm^{-1} (C=O) decreased and almost disappeared after alkaline treatment due to acetate elimination.

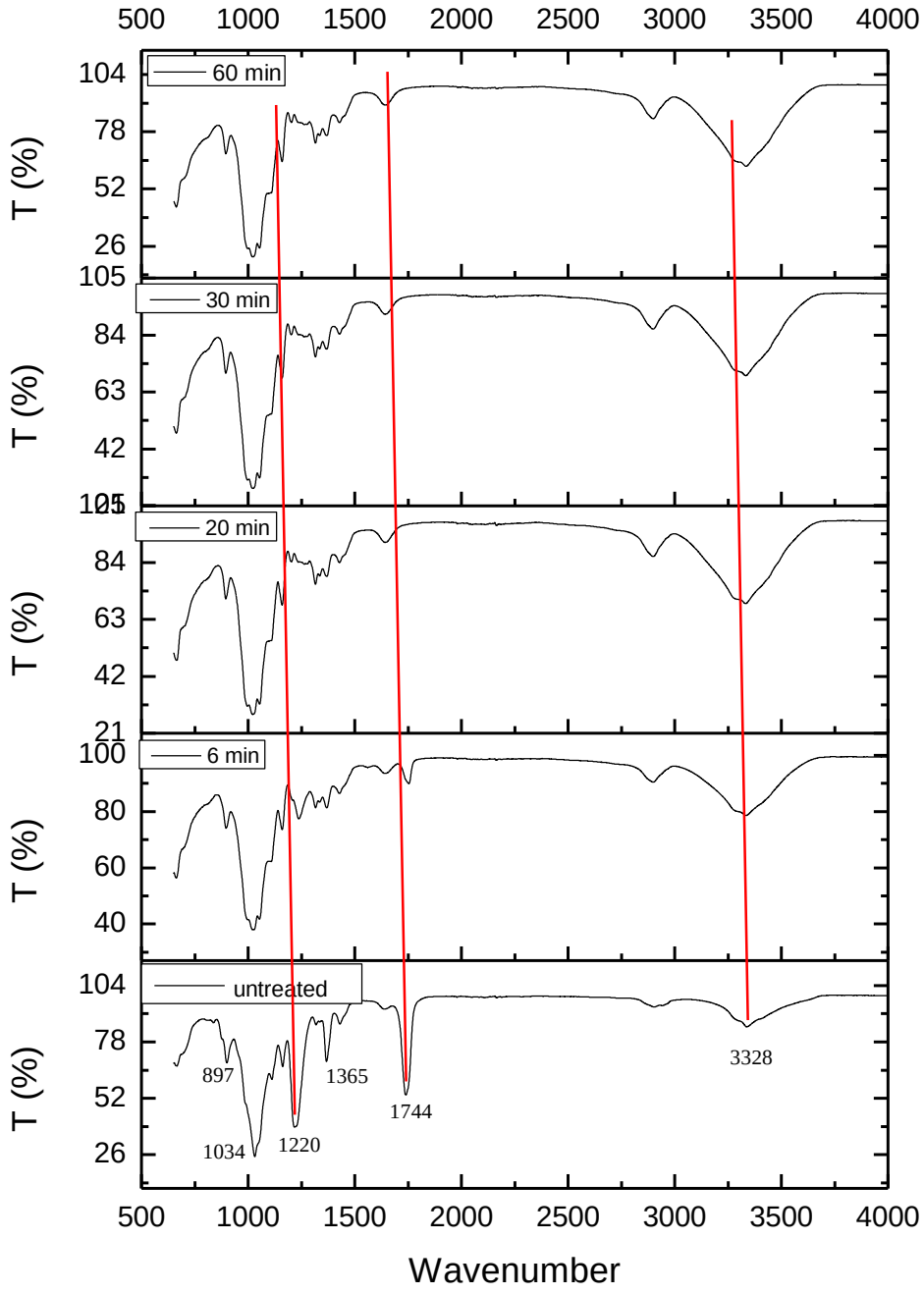

268

269 **Figure 4**. FTIR spectra of CTA/CNCs nanocomposite film membranes at different time of alkaline

270 treatment, a) Wavenumber range in 2,000 – 4,000 cm^{-1}, b) Wavenumber range in 600 to 2,200 cm^{-1}.

271

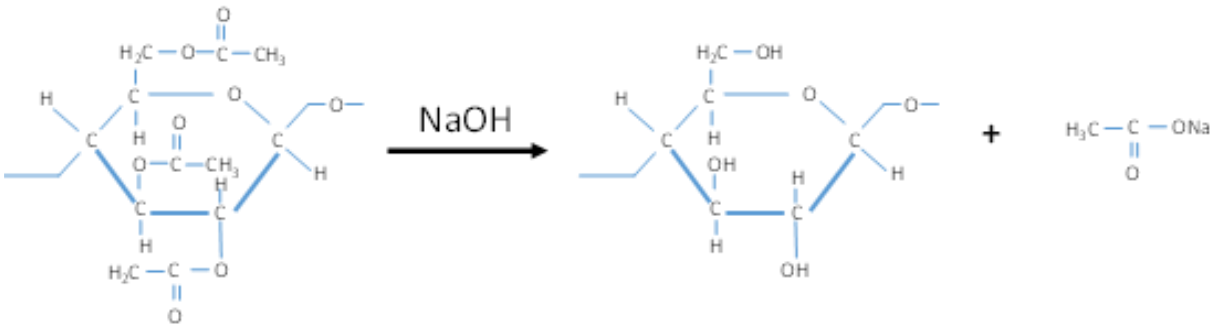

Figure 5. Deacetylation of cellulose triacetate with NaOH

3.1.4. Water uptake measurement

Water uptake was measured to investigate the effect of alkaline treatment on the water absorption of the CTA/CNCs nanocomposite film membrane. Figure 6 reveals that alkaline treatment of the CTA/CNCs nanocomposite film membrane significantly enhances the absorption of water. Figure 6 shows that water uptake increased drastically by 421% after 6 minutes of alkaline treatment compared to the untreated film membrane . A further increase of the alkaline treatment time to 20, 30 and 60 minutes only increased the water uptake by 36%, 24% and 13%, respectively. The large improvement of water uptake indicates that the alkaline treatment has a positive impact on altering the hydrophilicity of the CTA/CNCs nanocomposite film membrane. Longer alkaline treatment times resulted in an increasing water uptake of the nanocomposite film membranes. This is also confirmed by FTIR results, as shown in Figure 4: an increasing time of alkaline treatment enhances the O-H groups, which leads to an improvement of membrane hydrophilicity.

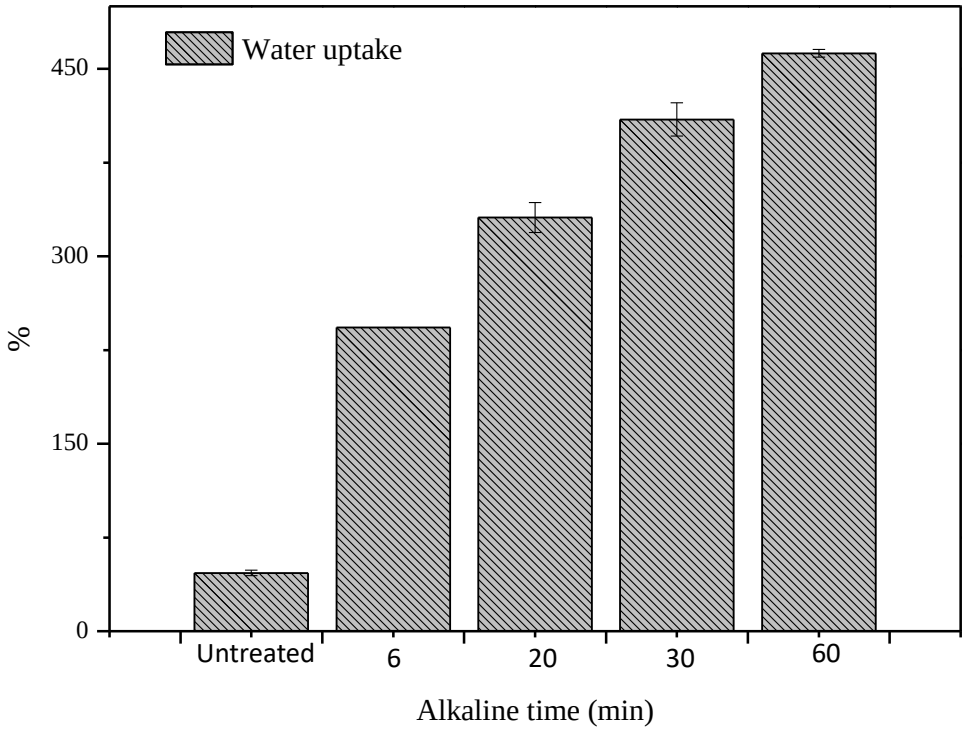

Figure 6. Water uptake the film membranes at different time of alkaline treatment.

3.1.5. Contact angle

The increase of membrane surface hydrophilicity after the alkaline treatment was also characterized by contact angle measurement. Figure 7 shows that the film membrane contact angle decreased from 65.6° to 26.3° after only 6 minutes of alkaline treatment. On the other hand, there was no significant decrease in contact angle when the alkaline time was increased from 6 to 30 minutes (26.3° to 24.7°). The decreasing contact angle to 26.27° and 24.7° indicates that alkaline treatment is a very effective method to enhance the surface hydrophilicity of the CTA/CNCs nanocomposite film membranes.

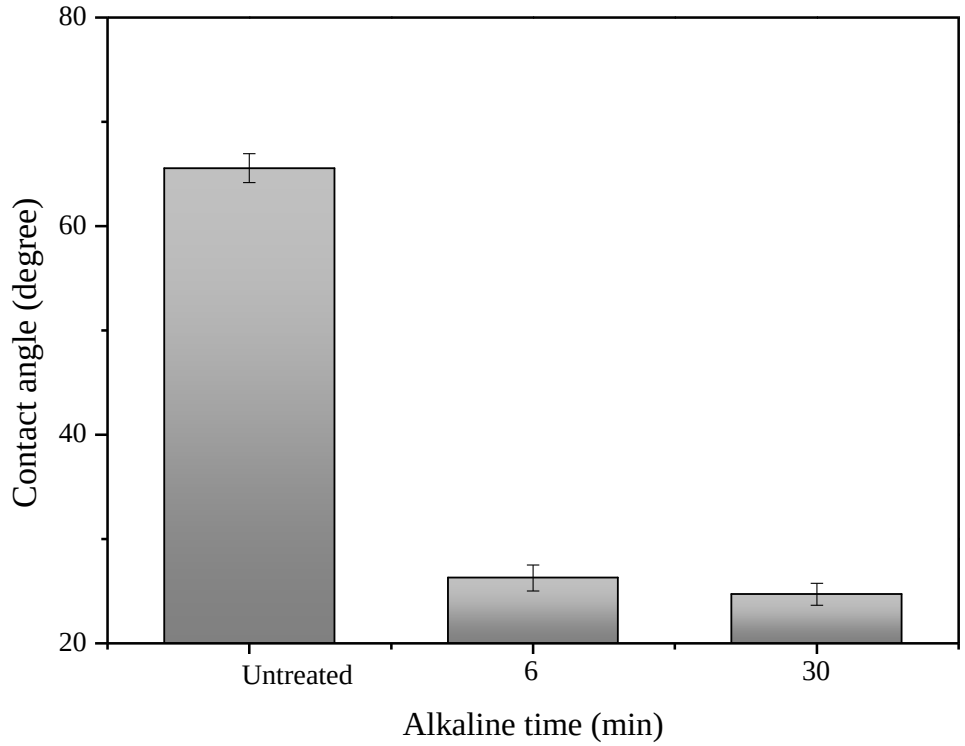

Figure 7. Contact angle at different time of alkaline treatment.

3.2. Performance of CTA/CNCs nanocomposite film membranes in PV desalination

3.2.1. Effect of time of alkaline treatment on membrane performance

The influence of the alkaline treatment time on the pervaporation performance of the CTA/CNCs nanocomposite film membranes in desalination is shown in Figure 8. The water flux of the nanocomposite film membranes can be significantly improved by simply controlling the alkaline treatment period. The water flux enhanced from 3.6 $kg.m^{-2}.h^{-1}$ to 24 $kg.m^{-2}.h^{-1}$ (567%) when the CTA/CNCs nanocomposite film membrane was treated in NaOH solution for 6 minutes with an intact salt rejection, maintaining at 99.9%. The water flux was further increased by 347%, from 24 $kg.m^{-2}.h^{-1}$ to 107.5 $kg.m^{-2}.h^{-1}$, when the alkaline treatment was prolonged from 6 minutes to 30 minutes with salt rejection kept of 99.9 %. This considerable water flux increase can be

attributed to the increase of the membrane hydrophilicity, as evidenced by water uptake measurements and the increase in hydrophilic functional groups measured by FTIR. This, in turn, will enhance the mass transport rate of water molecules inside nanocomposite film membranes during pervaporation. Increasing the alkaline treatment time beyond 30 minutes had a very small effect on the water flux. In fact, a decreasing salt selectivity was observed when 60 minutes alkaline treatment time was employed. This remarkable flux and salt selectivity can be attributed to the dense structure of the film membrane surface after the alkaline treatment with improved hydrophilic character of the film mmbranes.

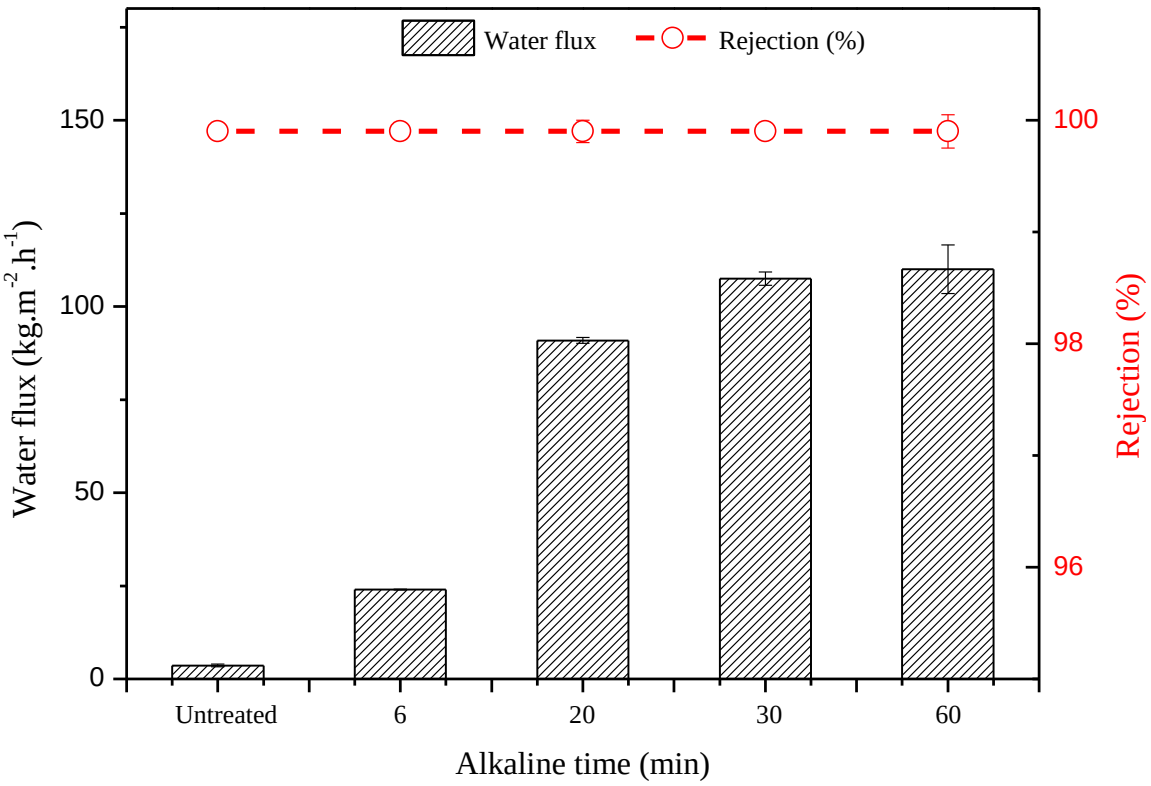

Figure 8. Pervaporation performance of CTA/CNCs nanocomposite film membrane at different times of alkaline treatment.

3.2.2. Effect of feed temperature on membrane performance

The effect of feed temperature on the pervaporation performance was investigated in the range 25 – 70 °C, as shown in Figure 9. It can be seen that rising the feed temperature from 25 to 70 °C results in an increase of water flux from 16 $kg.m^{-2}.h^{-1}$ to 107.5 $kg.m^{-2}.h^{-1}$ without significantly compromising the film membrane salt selectivity as the salt rejection was maintained at 99.9%. The increasing water flux is not surprising; the driving force in pervaporation process is the difference of partial vapor pressure between the feed and permeate side, as predicted by the Antoine equation [29]. As the partial vapor pressure of the permeate side is held constant, changing the partial vapor pressure at the feed side will lead to a change in driving force [30]. Furthermore, a higher temperature results in a higher water diffusivity [31], leading to a faster water transport rate inside the membranes.

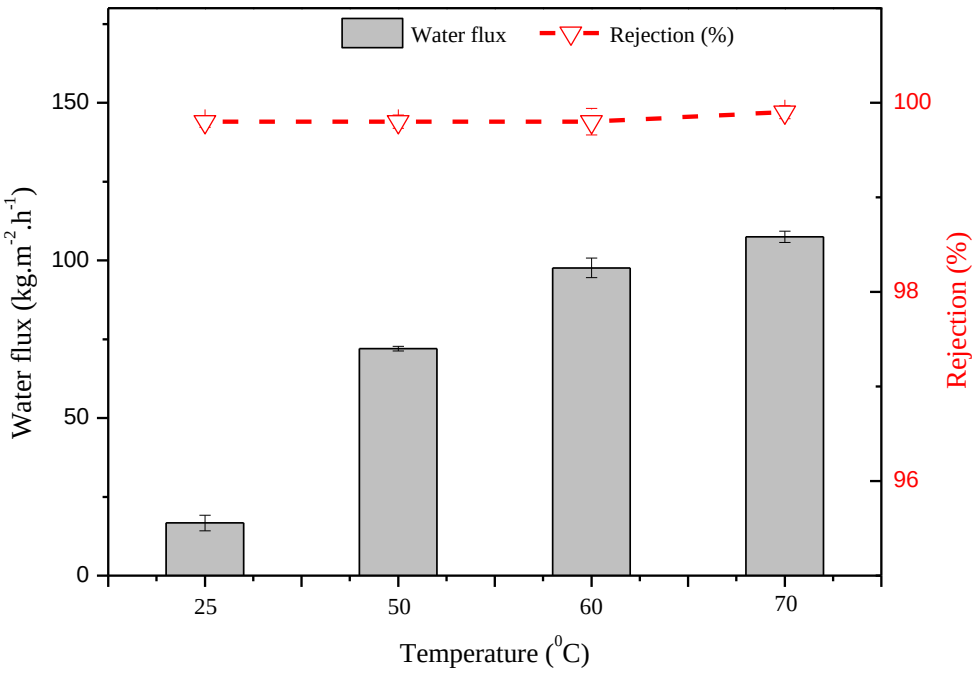

Figure 9. Pervaporation performance of CTA/CNCs nanocomposite film membrane (30 minutes in alkali treatment) at different temperatures.

Theoretically, the relationship of water flux with operating temperature can be explained by the Arrhenius equation [32]–[34].

$$J_i = J_o \exp\left(-\frac{E_{p,i}}{RT}\right) \quad (4)$$

where J_i is the water flux of i, J_o is the pre-exponential factor, R is the gas constant, T is the absolute temperature and $E_{p,i}$ is the apparent activation energy for permeation. Figure 10 depicts the Arrhenius correlation, which shows the logarithmic relation between the water fluxes and the reciprocal operating temperatures. The water activation energy is 37.8 kJ mol^{-1}; the positive value of the activation energy indicates that the water flux enhances with temperature at the feed side [35].

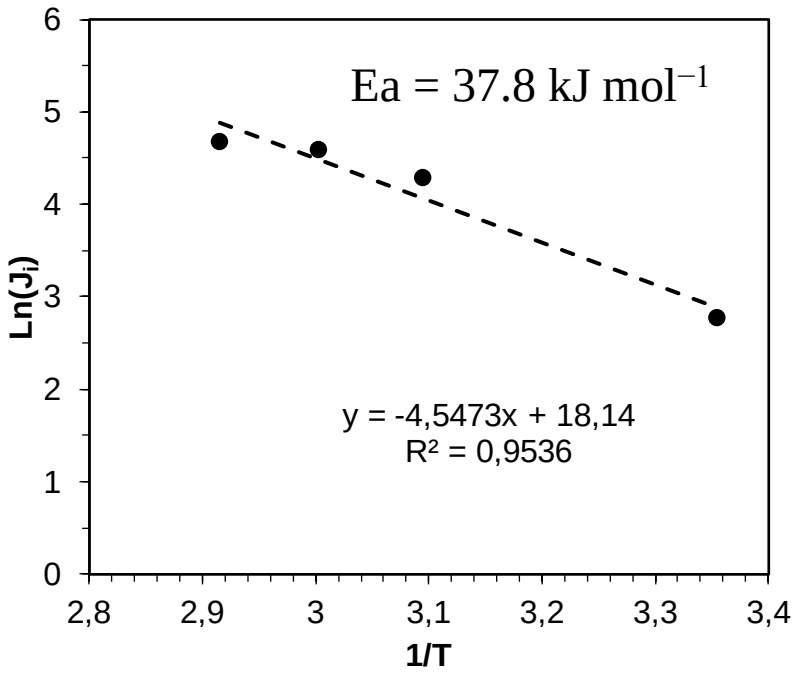

Figure 10. Arrhenius plot of ln (Ji) and 1000/T of CTA/CNCs nanocomposite film membrane (30 minutes in alkaline treatment)

3.2.3. Performance of CTA/CNCs at different feed concentrations

Figure 11 shows the effect of the NaCl concentration in the feed solution on the

355 pervaporation performance. It can be seen that adding 90 g/L of NaCl in the pure water of feed
356 solution decreases the water flux by 31.5%, from 157 $k.m^{-2}.h^{-1}$ to 107.5 $k.m^{-2}.h^{-1}$. While increasing
357 NaCl concentration from 90 g/L to 200 g/L decreases the water flux. decreases the water flux by
358 45.5% from 107.5 $k.m^{-2}.h^{-1}$ to 58.5 $kg.m^{-2}.h^{-1}$, however, the salt rejection is still kept at 99.9%. It
359 has been reported in the literature that the feed concentration directly affects the sorption of the
360 species at the membrane surface [33]. Increasing the NaCl concentration from 9 wt.% to 20 wt.%
361 corresponds to a reduction of the water concentration from 91 wt.% to 80 wt.%, which
362 subsequently reduces the sorption of water molecules at the membrane interface [36]. This causes
363 the water diffusion crossing the membrane to decrease, leading to a reduction in the water flux. As
364 30 minutes alkaline treatment resulted in optimized membrane performance, this film membrane
365 was further evaluated for 12 h pervaporation desalination with 90 g/L and 200 g/L of NaCl as the
366 feed solutions. Figure 12 reveals that a stable film membrane water flux can be obtained with a
367 stable salt rejection in the range of 99.8 – 99.9%. Subsequently, this promising membrane
368 performance will be suitable to treat feed solutions with hypersaline conditions.

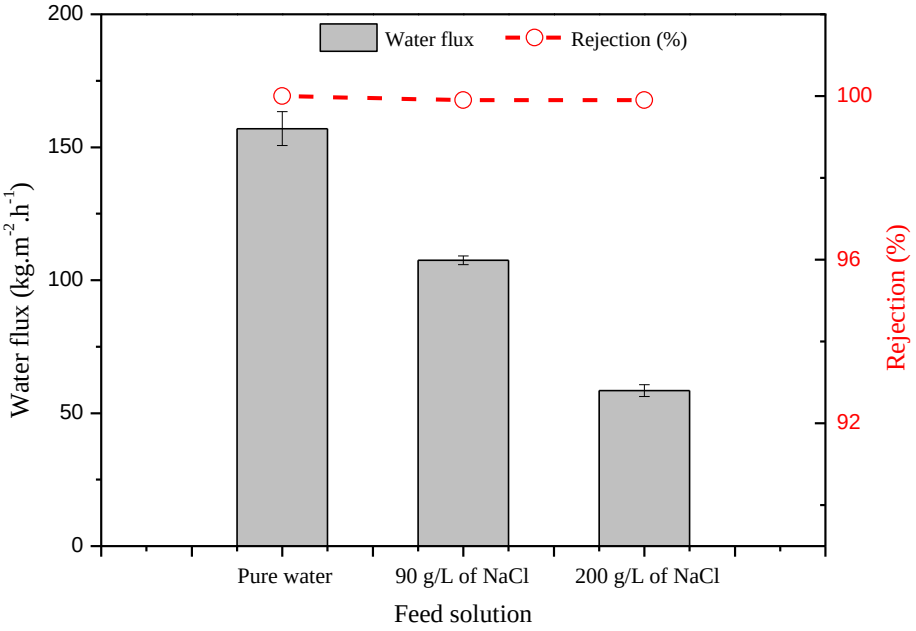

Figure 11. Pervaporation performance of CTA/CNCs nanocomposite film membrane (30 minutes in alkali treatment) at different NaCl concentrations

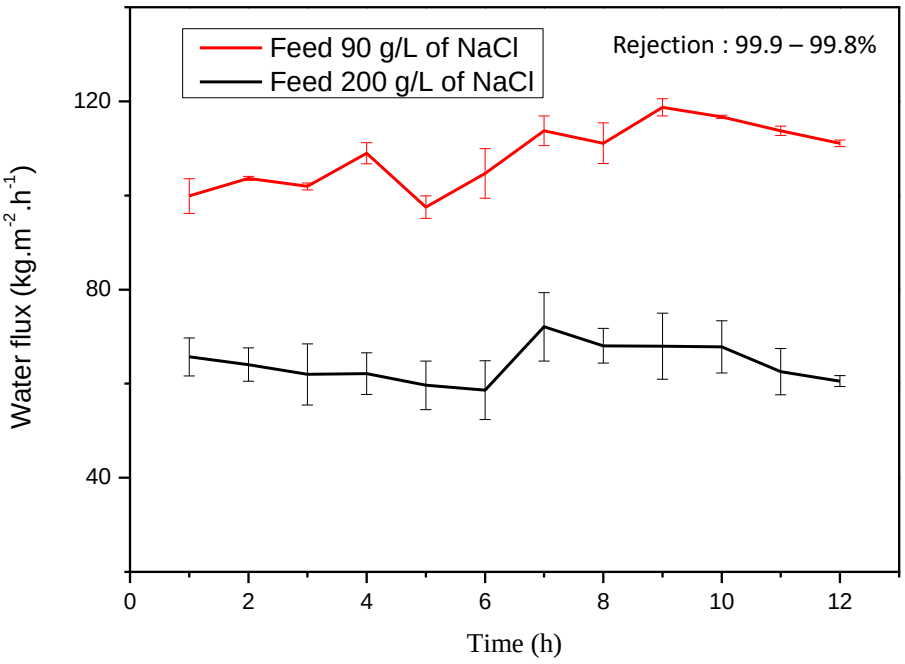

373 **Figure 12**. Pervaporation performance of CTA/CNCs nanocomposite film membrane (30 minutes
374 in alkali treatment) at different NaCl concentrations during 12 h pervaporation process.
375
376 Driving force for pervaporation desalination relies on the chemical potential gradient
377 between the feed side and permeate side of the membrane[37], [38] which the concentration
378 gradient could be expressed in terms of partial vapor pressure [39]. Currently, pervaporation is a
379 growing interest in applying to treat hypersaline feeds. Table 1 compares the recently developed
380 pervaporation membranes for hypersaline feed conditions.

381 **Table 1**. Summary of the recently developed pervaporation desalination membranes

Membranes	Feed concentration (g/L)	Operating temperature (°C)	Flux ($kg.m^{-2}.h^{-1}$)	Rejection (%)	Ref.
CTA/CNCs	90	70	7.6	99.7	[22]
CTA/Al_2O_3	90	70	5.0	99.8	[17]
CTA/Ludox-SiO_2	60	70	4.8	99.8	[40]
sPEEK/PES	100	70	4.9	>99.97	[41]
PA/GO	100	70	24	99.99	[42]
MAX-MXene	35	30	22.8	>99.7	[43]
GO-PVA	100	85	98.0	99.99	[44]
PVA/P(AA-AMPS)	200	75	74.1	99.7	[45]
PVA/silicate nanoclay	100	40	21.1	~99.99	[46]
LbL PEI/GO	200	65	8.4	99.9	[47]
PVA/GA/Laponite	100	70	39.9	99.9	[48]
Alkali treated CTA/CNCs	90	70	107.5	>99.8	This work

	200	70	58.5	>99.8	This work

4. Conclusion

Alkaline treatment of a CTA/CNCs nanocomposite membrane results in an enhancement of the pervaporation desalination performance. Alkaline treatment does not significantly change the membrane surface morphology. Hence, the salt rejection is still maintained above 99%. Alkaline treatment generates a gelation process on the membrane and improves the hydrophilicity, which leads to an increased water flux. The optimum time of alkaline treatment is 30 minutes at operating temperature of 70 ^{o}C with an increase of water flux from 3.6 $kg.m^{-2}.h^{-1}$ to 107.5 $kg.m^{-2}.h^{-1}$ for a feed solution of 90 g/L NaCl. For 200 g/L of NaCl in the feed solution, the water flux is 58.5 $kg.m^{-2}.h^{-1}$. Alkaline treatment of the CTA/CNCs nanocomposite membrane allows to maintain a high salt rejection, above 99.8%, at hypersaline feed conditions. This work shows that a simple alkaline treatment of CTA/CNCs nanocomposite membranes can be a tool to enhance the performance of this class of pervaporation desalination membranes with a promising capability to treat hypersaline feed solutions in a very efficient way.

Declaration of competing interest

The authors declare there are no competing interests.

Acknowledgment

This research was supported by the Indonesia Endowment Fund for Education (LPDP). The authors would like to thank to Chritine wouters (KU Leuven) for measuring FTIR.

References

[1] J. M. Gordon and T. C. Hui, “Thermodynamic perspective for the specific energy consumption of seawater desalination,” *Desalination*, vol. 386, pp. 13–18, 2016.

[2] Y. Hartanto, M. Corvilain, H. Mariën, J. Janssen, and I. F. J. Vankelecom, “Interfacial polymerization of thin-film composite forward osmosis membranes using ionic liquids as organic reagent phase,” *J. Memb. Sci.*, vol. 601, p. 117869, 2020.

[3] Y. Li, E. Wong, Z. Mai, and B. Van der Bruggen, “Fabrication of composite polyamide/Kevlar aramid nanofiber nanofiltration membranes with high permselectivity in water desalination,” *J. Memb. Sci.*, vol. 592, p. 117396, 2019.

[4] Z. Ali *et al.*, “Defect-free highly selective polyamide thin-film composite membranes for desalination and boron removal,” *J. Memb. Sci.*, vol. 578, pp. 85–94, 2019.

[5] S. Lee, J. Choi, Y.-G. Park, H. Shon, C. H. Ahn, and S.-H. Kim, “Hybrid desalination processes for beneficial use of reverse osmosis brine: Current status and future prospects,” *Desalination*, vol. 454, pp. 104–111, 2019.

[6] D. M. Davenport, A. Deshmukh, J. R. Werber, and M. Elimelech, “High-Pressure Reverse Osmosis for Energy-Efficient Hypersaline Brine Desalination: Current Status, Design Considerations, and Research Needs,” *Environ. Sci. Technol. Lett.*, vol. 5, no. 8, pp. 467–475, Aug. 2018.

[7] R. K. McGovern and J. H. Lienhard V, “On the potential of forward osmosis to energetically outperform reverse osmosis desalination,” *J. Memb. Sci.*, vol. 469, pp. 245–250, 2014.

[8] K. J. Lu, Y. Chen, and T.-S. Chung, “Design of omniphobic interfaces for membrane distillation – A review,” *Water Res.*, vol. 162, pp. 64–77, 2019.

[9] G. Liu *et al.*, “Ultrathin two-dimensional MXene membrane for pervaporation desalination,” *J. Memb. Sci.*, vol. 548, pp. 548–558, 2018.

[10] V. S. S. L. P. Talluri, A. Tleuova, S. Hosseini, and O. Vopicka, “Selective separation of 1-butanol from aqueous solution through pervaporation using PTSMP-silica nano hybrid membrane,” *Membranes (Basel).*, vol. 10, no. 4, 2020.

[11] N. Jullok *et al.*, “Effect of silica nanoparticles in mixed matrix membranes for pervaporation dehydration of acetic acid aqueous solution: plant-inspired dewatering systems,” *J. Clean. Prod.*, vol. 112, pp. 4879–4889, 2016.

[12] K.-F. Chen, P.-Y. Zheng, J.-K. Wu, N.-X. Wang, Q.-F. An, and K.-R. Lee, “Polyelectrolyte complexes/silica hybrid hollow fiber membrane for fusel oils pervaporation dehydration processes,” *J. Memb. Sci.*, vol. 545, pp. 284–291, 2018.

[13] X.-W. Liu *et al.*, “High-performance polyamide/ceramic hollow fiber TFC membranes with TiO2 interlayer for pervaporation dehydration of isopropanol solution,” *J. Memb. Sci.*, vol. 576, pp. 26–35, 2019.

[14] E. Ataeivarjovi, Z. Tang, J. Chen, Z. Zhao, and G. Dong, “Enhancement of CO2 Desorption from a Novel Absorbent (Dimethyl Carbonate) by Using a PDMS/TiO2 Pervaporation Membrane,” *ACS Sustain. Chem. Eng.*, vol. 7, no. 14, pp. 12125–12137, Jul. 2019.

[15] J. H. Jhaveri, C. M. Patel, and Z. V. P. Murthy, “Preparation, characterization and application of GO-TiO2/PVC mixed matrix membranes for improvement in performance,” *J. Ind. Eng. Chem.*, vol. 52, pp. 138–146, 2017.

[16] K. Knozowska, G. Li, W. Kujawski, and J. Kujawa, “Novel heterogeneous membranes for enhanced separation in organic-organic pervaporation,” *J. Memb. Sci.*, vol. 599, p. 117814, 2020.

[17] I. Prihatiningtyas, G. A. Gebreslase, and B. Van der Bruggen, “Incorporation of Al2O3 into

cellulose triacetate membranes to enhance the performance of pervaporation for desalination of hypersaline solutions," *Desalination*, vol. 474, p. 114198, 2020.

[18] L. Li, J. Hou, and V. Chen, "Pinning Down the Water Transport Mechanism in Graphene Oxide Pervaporation Desalination Membranes," *Ind. Eng. Chem. Res.*, vol. 58, no. 10, pp. 4231–4239, Mar. 2019.

[19] R. Castro-Muñoz *et al.*, "Towards the dehydration of ethanol using pervaporation cross-linked poly(vinyl alcohol)/graphene oxide membranes," *J. Memb. Sci.*, vol. 582, pp. 423–434, 2019.

[20] W. Tang, H. Lou, Y. Li, X. Kong, Y. Wu, and X. Gu, "Ionic liquid modified graphene oxide-PEBA mixed matrix membrane for pervaporation of butanol aqueous solutions," *J. Memb. Sci.*, vol. 581, pp. 93–104, 2019.

[21] I. Prihatiningtyas, A. Volodin, and B. Van Der Bruggen, "110th Anniversary: Cellulose Nanocrystals as Organic Nanofillers for Cellulose Triacetate Membranes Used for Desalination by Pervaporation," *Ind. Eng. Chem. Res.*, vol. 58, no. 31, pp. 14340–14349, 2019.

[22] I. Prihatiningtyas, Y. Li, Y. Hartanto, A. Vananroye, N. Coenen, and B. Van der Bruggen, "Effect of solvent on the morphology and performance of cellulose triacetate membrane/cellulose nanocrystal nanocomposite pervaporation desalination membranes," *Chem. Eng. J.*, vol. 388, 2020.

[23] A. Wittmar, H. Thierfeld, S. Köcher, and M. Ulbricht, "Routes towards catalytically active TiO2 doped porous cellulose," *RSC Adv.*, vol. 5, no. 45, pp. 35866–35873, 2015.

[24] L. C. Malucelli, D. Lomonaco, M. A. S. C. Filho, and W. L. E. Magalhães, "Cellulose triacetate from different sources: Modification assessment through thermal and chemical characterization," *Holzforschung*, vol. 74, no. 5, pp. 505–512, 2020.

[25] G. Bali, X. Meng, J. I. Deneff, Q. Sun, and A. J. Ragauskas, "The effect of alkaline pretreatment methods on cellulose structure and accessibility," *ChemSusChem*, vol. 8, no. 2, pp. 275–279, 2015.

[26] E. Xu, D. Wang, and L. Lin, "Chemical structure and mechanical properties of wood cellwalls treated with acid and alkali solution," *Forests*, vol. 11, no. 1, 2020.

[27] B. W. Chieng, S. H. Lee, N. A. Ibrahim, Y. Y. Then, and Y. Y. Loo, "Isolation and characterization of cellulose nanocrystals from oil palm mesocarp fiber," *Polymers (Basel).*, vol. 9, no. 8, pp. 1–11, 2017.

[28] E. B. C. Santos *et al.*, "Effect of alkaline and hot water treatments on the structure and morphology of piassava fibers," *Mater. Res.*, vol. 21, no. 2, pp. 1–11, 2018.

[29] D. U. Lawal and A. E. Khalifa, "Flux Prediction in Direct Contact Membrane Distillation," *Int. J. Mater. Mech. Manuf.*, vol. 2, no. 4, pp. 302–308, 2014.

[30] Z. Xie, D. Ng, M. Hoang, T. Duong, and S. Gray, "Separation of aqueous salt solution by pervaporation through hybrid organic-inorganic membrane: Effect of operating conditions," *Desalination*, vol. 273, no. 1, pp. 220–225, 2011.

[31] A. Svang-Ariyaskul *et al.*, "Blended chitosan and polyvinyl alcohol membranes for the pervaporation dehydration of isopropanol," *J. Memb. Sci.*, vol. 280, no. 1, pp. 815–823, 2006.

[32] C. K. Yeom and K.-H. Lee, "Vapor permeation of ethanol-water mixtures using sodium

alginate membranes with crosslinking gradient structure," *J. Memb. Sci.*, vol. 135, no. 2, pp. 225–235, 1997.

[33] R. Jiraratananon, A. Chanachai, R. Y. M. Huang, and D. Uttapap, "Pervaporation dehydration of ethanol–water mixtures with chitosan/hydroxyethylcellulose (CS/HEC) composite membranes: I. Effect of operating conditions," *J. Memb. Sci.*, vol. 195, no. 2, pp. 143–151, 2002.

[34] F. Peng, L. Lu, H. Sun, and Z. Jiang, "Analysis of annealing effect on pervaporation properties of PVA-GPTMS hybrid membranes through PALS," *J. Memb. Sci.*, vol. 281, no. 1, pp. 600–608, 2006.

[35] A. A. Kittur, M. Y. Kariduraganavar, U. S. Toti, K. Ramesh, and T. M. Aminabhavi, "Pervaporation separation of water–isopropanol mixtures using ZSM-5 zeolite incorporated poly(vinyl alcohol) membranes," *J. Appl. Polym. Sci.*, vol. 90, no. 9, pp. 2441–2448, Nov. 2003.

[36] D. Wu, A. Gao, H. Zhao, and X. Feng, "Pervaporative desalination of high-salinity water," *Chem. Eng. Res. Des.*, vol. 136, pp. 154–164, 2018.

[37] C. S. Slater, T. Schurmann, J. MacMillian, and A. Zimarowski, "Separation of diacteone alcohol-water mixtures by membrane pervaporation," *Sep. Sci. Technol.*, vol. 41, no. 12, pp. 2733–2753, 2006.

[38] C. Cannilla, G. Bonura, and F. Frusteri, "Potential of pervaporation and vapor separation with water selective membranes for an optimized production of biofuels—a review," *Catalysts*, vol. 7, no. 6, 2017.

[39] A. C. M. Franken, M. H. V. Mulder, and C. A. Smolders, "Pervaporation process using a thermal gradient as the driving force," *J. Memb. Sci.*, vol. 53, no. 1–2, pp. 127–141, 1990.

[40] I. Prihatiningtyas, Y. Hartanto, M. S. R. Ballesteros, and B. Van der Bruggen, " Cellulose triacetate/ LUDOX-SiO 2 nanocomposite for synthesis of pervaporation desalination membranes ," *J. Appl. Polym. Sci.*, no. September, p. 50000, 2020.

[41] H. Zeng *et al.*, "Hydrophilic SPEEK/PES composite membrane for pervaporation desalination," *Sep. Purif. Technol.*, vol. 250, p. 117265, 2020.

[42] X. Zhao, Z. Tong, X. Liu, J. Wang, and B. Zhang, "Facile Preparation of Polyamide–Graphene Oxide Composite Membranes for Upgrading Pervaporation Desalination Performances of Hypersaline Solutions," *Ind. Eng. Chem. Res.*, vol. 59, no. 26, pp. 12232–12238, Jul. 2020.

[43] M. Ding *et al.*, "2D laminar maleic acid-crosslinked MXene membrane with tunable nanochannels for efficient and stable pervaporation desalination," *J. Memb. Sci.*, vol. 600, p. 117871, 2020.

[44] J. Sun, X. Qian, Z. Wang, F. Zeng, H. Bai, and N. Li, "Tailoring the microstructure of poly(vinyl alcohol)-intercalated graphene oxide membranes for enhanced desalination performance of high-salinity water by pervaporation," *J. Memb. Sci.*, vol. 599, p. 117838, 2020.

[45] Y. L. Xue, J. Huang, C. H. Lau, B. Cao, and P. Li, "Tailoring the molecular structure of crosslinked polymers for pervaporation desalination," *Nat. Commun.*, vol. 11, no. 1, 2020.

[46] M. A. Selim, A. J. Toth, D. Fozer, E. Haaz, and P. Mizsey, "Pervaporative desalination of concentrated brine solution employing crosslinked PVA/silicate nanoclay membranes,"

Chem. Eng. Res. Des., vol. 155, pp. 229–238, 2020.

[47] E. Halakoo and X. Feng, "Layer-by-layer assembly of polyethyleneimine/graphene oxide membranes for desalination of high-salinity water via pervaporation," *Sep. Purif. Technol.*, vol. 234, p. 116077, 2020.

[48] A. Selim *et al.*, "Preparation and characterization of PVA/GA/Laponite membranes to enhance pervaporation desalination performance," *Sep. Purif. Technol.*, vol. 221, pp. 201–210, 2019.

https://pervaporation-membranes.com/home/introduction-to-pervaporation-and-vapor-permeation/

Graphical abstract